

# HADS-Net: A Hybrid Attention-Augmented Dual-Stream Network with Physics-Informed Augmentation for Breast Ultrasound Image Classification

<sup>1</sup>Chinedu Emmanuel Mbonu, <sup>2</sup>Blessing Nwamaka Iduh, <sup>3</sup>Joseph Ikechukwu Odo, <sup>4</sup>Doris Chinedu Asogwa

<sup>1</sup>Department of Computer Science, Nazarbayev University, Astana

<sup>1,2,4</sup>Department of Computer Science, Nnamdi Azikiwe University Awka, Nigeria

<sup>3</sup>Department of Computer Science, Peter University Achina-Onneh, Nigeria

{ce.mbonu [ @nu.edu.kz, @unizik.edu.ng ], bn.iduh@unizik.edu.ng, ji.odo@puni.edu.ng, dc.asogwa@unizik.edu.ng }

**Abstract**—Accurate classification of breast ultrasound images into benign, malignant, and normal categories is a critical yet challenging clinical task owing to low image contrast, inherent speckle noise, and significant inter-class visual ambiguity. Existing deep learning approaches predominantly rely on single-stream architectures trained with generic photographic augmentation strategies that fail to account for the physical properties of ultrasound image formation. In this work, we propose HADS-Net, a Hybrid Attention-Augmented Dual-Stream Network that simultaneously exploits global texture features and local lesion boundary cues through two complementary processing pathways. Stream 1 applies physics-informed augmentation simulating real ultrasound acquisition artefacts including speckle noise, acoustic shadowing, and gain variation before feeding images through a pretrained EfficientNet-B3 backbone projected to a 512-dimensional feature space. Stream 2 extracts Sobel edge maps to highlight lesion contours, processes them through a custom lightweight convolutional neural network, and projects the resulting 256-dimensional features to the same 512-dimensional space. A novel cross-attention fusion module then allows the texture stream to selectively query boundary features, producing a jointly optimised representation passed to a multi-layer perceptron classifier trained with an adaptive class-weighted focal loss. Five-fold stratified cross-validation with cosine annealing learning rate scheduling is employed, and the globally best checkpoint selected by lowest validation loss across all folds and epochs is evaluated on a held-out test set. On the publicly available Breast Ultrasound Images (BUSI) dataset, HADS-Net achieves a test accuracy of 96.58%, a macro ROC-AUC of 0.9978, and a macro F1-score of 0.9654, outperforming state-of-the-art methods. These results demonstrate that modality-specific augmentation combined with cross-modal attention fusion constitutes an effective and generalisable framework for ultrasound-based breast cancer diagnosis. The implementation is publicly available on Github via <https://github.com/NedumCares/BIUS-Classification>

**Index Terms**—breast cancer, ultrasound imaging, dual-stream network, cross-attention, physics-informed augmentation, EfficientNet, focal loss, deep learning, BUSI dataset

## I. INTRODUCTION

Breast cancer remains the most prevalent malignancy among women globally, accounting for approximately 30% of all new female cancer diagnoses annually [1]. Early and accurate

diagnosis is one of the important factors in improving patient outcomes and enabling less invasive treatment [3]. Ultrasound (US) imaging is among the most widely deployed screening modalities for breast lesions owing to its non-ionising nature, real-time capability, low cost, and absence of radiation exposure [4]. However, interpreting breast ultrasound images is inherently challenging: speckle noise, acoustic shadowing, varying gain settings, and the subtle visual similarity between benign and malignant lesions all contribute to significant intra- and inter-observer variability [5], [10].

Deep learning has emerged as a powerful approach to automating breast lesion classification. Ashraf et al. [3] demonstrated on the BUSI dataset that ResNet50 achieves 85% accuracy and InceptionV3 achieves 84% with standard transfer learning, while MobileNetV2 reached only 50%, highlighting the strong dependence of performance on architectural depth. Deb and Jha [5] proposed a fuzzy-rank-based ensemble of four CNNs on BUSI, achieving  $85.23 \pm 2.52\%$  accuracy with five-fold cross-validation and outperforming each individual base learner. Gheflati and Rivaz [6] evaluated Vision Transformer (ViT) architectures on BUSI for the first time, reporting that ResNet50 is the strongest CNN baseline at 85.3% accuracy and 0.95 AUC. Ashraf et al. [3] further showed that ViT-B32 fine-tuned on BUSI achieves 95% accuracy, a 10-percentage-point improvement over the best CNN baseline. Pacal [7] conducted a systematic benchmark of multiple architectures on BUSI, finding that a Vision Transformer achieves 88.6% accuracy and EfficientNet reaches 85.6%. Islam et al. [9] proposed an Ensemble Deep Convolutional Neural Network (EDCNN) combining MobileNet and Xception, achieving 87.82% accuracy and AUC of 0.91 on BUSI. Alotaibi et al. [8] applied a three-step preprocessing scheme (speckle filtering, ROI highlighting, RGB fusion) with VGG19 transfer learning, achieving 87.8% accuracy on BUSI. Asif et al. [11] proposed a feature fusion and CBAM attention framework using MobileNetV2 and DenseNet121, reporting an AUC of 0.9834 on the BUSI multi-class dataset.

Despite these advances, three fundamental limitations persist. First, most existing methods apply generic photographic augmentation that does not model the physics of ultrasound acquisition. Speckle noise, acoustic shadowing, and time-gain compensation (TGC) variation are intrinsic artifacts inherent in clinical ultrasound images and represent real sources of domain shift in deployment. Second, Byra et al. [4] demonstrated through class activation map analysis that deep networks primarily attend to the peritumoral boundary region (38% of correctly classified cases) more than any other region, confirming that lesion boundary features are the most diagnostically significant visual cue. To the best of our knowledge no prior method dedicates a separate processing stream to explicitly modelling boundary information. Third, no prior work applies cross-attention between complementary image representations, texture and boundary to achieve selective, dynamic feature integration.

To address these three gaps, we propose HADS-Net (Hybrid Attention-Augmented Dual-Stream Network) with four contributions:

- 1) **Physics-Informed Augmentation:** A modality-specific pipeline simulating speckle noise, acoustic shadowing, and gain variation artefacts intrinsic to ultrasound acquisition.
- 2) **Dual-Stream Architecture:** Stream 1 processes raw ultrasound images via pretrained EfficientNet-B3; Stream 2 processes Sobel edge maps via a lightweight CNN, explicitly encoding lesion boundary features.
- 3) **Cross-Attention Fusion:** A novel multi-head cross-attention module in which the texture stream queries the boundary stream, enabling selective integration of boundary cues based on texture context.
- 4) **Adaptive Class-Weighted Focal Loss:** Combines inverse-frequency class weights with focal down-weighting to address class imbalance in BUSI (benign:malignant:normal  $\approx$  3.3:1.6:1).

Evaluated on the publicly available BUSI dataset using five-fold stratified cross-validation and a held-out test set, HADS-Net demonstrates strong and well-calibrated classification performance across all three classes, achieving competitive results against state-of-the-art methods with balanced per-class performance for benign, malignant, and normal categories.

## II. RELATED WORK

### A. Traditional and CNN-Based Approaches

Before deep learning became dominant, breast ultrasound classification relied on handcrafted features such as GLCM texture descriptors and morphological shape statistics combined with SVMs or random forests [4]. While interpretable, such approaches required domain expertise and could not generalise across imaging equipment. Convolutional neural networks (CNNs) with transfer learning have since become the standard. Ashraf et al. [3] systematically compared MobileNetV2, ResNet50, and InceptionV3 on BUSI, finding that ResNet50 achieved the best CNN accuracy of 85% using the

Adam optimiser at  $10^{-5}$  learning rate. Pacal [7] conducted a broader benchmark including AlexNet (79.5%), VGG16 (85.4%), EfficientNet (85.6%), and multiple ResNet variants on BUSI, using the same SGD training protocol with ImageNet initialisation for all models.

### B. Ensemble and Feature Fusion Methods

Deb and Jha [5] proposed a fuzzy-rank-based ensemble combining four CNN base learners VGG-19, DenseNet, InceptionNet, and Xception pretrained on ImageNet with the last five layers fine-tuned. A fuzzy ranking scheme aggregated predictions from all four models. With five-fold CV on BUSI, individual learners achieved 77.69–83.23% accuracy, while the ensemble reached  $85.23 \pm 2.52\%$ , also outperforming majority voting (83.66%) and weighted majority voting (84.87%). Alotaibi et al. [8] proposed a three-step image preprocessing scheme speckle noise filtering via block-matching 3D filtering, ROI highlighting, and RGB fusion—applied before VGG19 transfer learning on BUSI and two additional datasets, achieving best BUSI accuracy of 87.8% and AUC of 0.9497 with five-fold cross-validation. Islam et al. [9] combined MobileNet and Xception in an EDCNN framework with Grad-CAM explainability, achieving 87.82% accuracy and AUC of 0.91 on BUSI. Asif et al. [11] fused features from MobileNetV2 and DenseNet121 using the Convolutional Block Attention Module (CBAM) and applied Grad-CAM, Saliency Maps, and SHAP for interpretability, reporting an AUC of 0.9834 on the BUSI multi-class dataset.

### C. Vision Transformer Architectures

Gheflati and Rivaz [6] were among the first to evaluate ViTs on BUSI, showing that ResNet50 remained the strongest CNN baseline at 85.3% accuracy and AUC 0.95, while ViT models demonstrated comparable or superior performance and used a weighted cross-entropy loss to address class imbalance. Ashraf et al. [3] showed that ViT-B32 achieves 95% validation accuracy on BUSI, outperforming the best CNN baseline by 10 percentage points. Pacal [7] further confirmed that a Vision Transformer achieves 88.6% accuracy the best result in their multi-model benchmark with an F1-score of 88.7%. Kiran et al. [13] proposed EfficientKNN, combining EfficientNetB3 feature extraction with a k-Nearest Neighbours classifier, achieving approximately 94% accuracy on BUSI with EfficientNetB3 alone reaching 90%.

### D. Explainability and Feature Localisation

Byra et al. [4] developed a ResNet-based classifier for breast mass classification with CAM-based saliency maps, using 272 masses (123 malignant, 149 benign) with a 204/68 train/test split. The model achieved AUC 0.887 and accuracy 0.835. The pointing game metric showed that 71% of network decisions corresponded to clinically relevant regions: the peritumoral boundary (38%), the mass interior (34%), and the region below the mass (30%). The dominance of boundary features directly motivates our explicit boundary processing stream. Alotaibi et al. [8], Islam et al. [9], and Asif et al. [11] all incorporated

Grad-CAM visualisation, collectively demonstrating a growing consensus on the importance of model interpretability in clinical ultrasound AI.

### E. Transfer Learning for Image Classification

Transfer learning with ResNet and EfficientNet architectures has shown strong generalisation across diverse classification tasks. Hossain et al. [12] applied VGG16 transfer learning with median filtering for speckle removal on combined breast ultrasound datasets (897 images), achieving 98.2% training accuracy and 91% testing accuracy with Grad-CAM localisation. Mbonu et al. [14] demonstrated that fine-tuned ResNet50 with five-fold cross-validation generalises reliably on small, imbalanced datasets, confirming that residual architectures and systematic cross-validation provide robust performance estimates across different image domains.

## III. PROPOSED METHODOLOGY

Fig. 1 illustrates the complete HADS-Net training pipeline.

### A. Dataset and Preprocessing

The BUSI dataset [2] comprises 780 ultrasound images from 600 female patients aged 25–75 years, categorised as benign (437, 56.0%), malignant (210, 26.9%), and normal (133, 17.1%). The dataset is stratified and split into a training set (85%,  $N = 663$ ) and a held-out test set (15%,  $N = 117$ : 66 benign, 31 malignant, 20 normal). All images are resized to  $224 \times 224$  pixels and normalised using ImageNet statistics ( $\mu = [0.485, 0.456, 0.406]$ ,  $\sigma = [0.229, 0.224, 0.225]$ ).

### B. Physics-Informed Augmentation

Standard natural-image augmentations do not capture the physics of ultrasound acquisition. HADS-Net introduces three clinically motivated augmentations applied stochastically at training time.

**Speckle noise:** Coherent scattering of ultrasound waves produces granular noise modelled as additive Gaussian noise:

$$I_{\text{speckle}}(x, y) = I(x, y) + \eta(x, y), \quad \eta \sim \mathcal{N}(0, \sigma_s^2) \quad (1)$$

where  $\sigma_s \in [0.05, 0.15] \times 255$ .

**Acoustic shadowing:** Highly reflective structures create dark vertical shadows simulated by:

$$I_{\text{shadow}}(x, y) = I(x, y) \cdot m(x), \quad m(x) = \begin{cases} \alpha & x \in [x_0, x_0 + w] \\ 1 & \text{otherwise} \end{cases} \quad (2)$$

where  $x_0$  is random,  $w = \lfloor 0.15W \rfloor$ , and  $\alpha \sim \mathcal{U}(0.2, 0.5)$ .

**Gain variation:** Operator-dependent time-gain compensation is simulated by:

$$I_{\text{gain}}(x, y) = I(x, y) \cdot g(y), \quad g(y) = g_{\min} + (g_{\max} - g_{\min}) \frac{y}{H} \quad (3)$$

with  $g_{\min} \sim \mathcal{U}(0.6, 0.9)$  and  $g_{\max} \sim \mathcal{U}(1.0, 1.3)$ .

One augmentation is selected uniformly with probability  $p = 1/3$ . Standard geometric augmentations (flip, rotate, elastic transform) are applied subsequently. Physics augmentation is disabled at validation and test time.

### C. Dual-Stream Architecture

**Stream 1 – Texture:** The augmented image is processed by pretrained EfficientNet-B3 [15], yielding  $\mathbf{f}_1 \in \mathbb{R}^{1536}$ , projected to a shared 512-d space:

$$\hat{\mathbf{f}}_1 = \text{ReLU}(W_1 \mathbf{f}_1 + b_1), \quad \hat{\mathbf{f}}_1 \in \mathbb{R}^{512} \quad (4)$$

**Stream 2 – Boundary:** The Sobel edge map is computed from the original image:

$$G_x = \begin{bmatrix} -1 & 0 & 1 \\ -2 & 0 & 2 \\ -1 & 0 & 1 \end{bmatrix} * I, \quad G_y = \begin{bmatrix} -1 & -2 & -1 \\ 0 & 0 & 0 \\ 1 & 2 & 1 \end{bmatrix} * I \quad (5)$$

$$E(x, y) = \sqrt{G_x(x, y)^2 + G_y(x, y)^2} \quad (6)$$

$E$  is processed by a four-stage lightweight CNN (channel depths 32, 64, 128, 256;  $3 \times 3$  convolutions, batch normalisation, ReLU, max-pooling), yielding  $\mathbf{f}_2 \in \mathbb{R}^{256}$ , projected to:

$$\hat{\mathbf{f}}_2 = \text{ReLU}(W_2 \mathbf{f}_2 + b_2), \quad \hat{\mathbf{f}}_2 \in \mathbb{R}^{512} \quad (7)$$

### D. Cross-Attention Fusion Module

The texture stream  $\hat{\mathbf{f}}_1$  queries the boundary stream  $\hat{\mathbf{f}}_2$  with  $H = 8$  attention heads and  $d_k = 64$ :

$$Q^{(h)} = W_Q^{(h)} \hat{\mathbf{f}}_1, \quad K^{(h)} = W_K^{(h)} \hat{\mathbf{f}}_2, \quad V^{(h)} = W_V^{(h)} \hat{\mathbf{f}}_2 \quad (8)$$

$$a^{(h)} = \frac{Q^{(h)} \cdot K^{(h)}}{\sqrt{d_k}}, \quad \tilde{a}^{(h)} = \text{softmax}(a^{(h)}) \quad (9)$$

$$\mathbf{z} = \text{LayerNorm} \left( W_O \left[ \bigoplus_{h=1}^H \tilde{a}^{(h)} V^{(h)} \right] + \hat{\mathbf{f}}_1 \right) \quad (10)$$

The residual connection ensures texture information is preserved when boundary features provide low signal.

### E. MLP Classifier

The fused vector  $\mathbf{z} \in \mathbb{R}^{512}$  is classified via:

$$\hat{y} = \text{softmax}(W_2 \cdot \text{ReLU}(W_1 \cdot \text{Dropout}(\mathbf{z}))) \quad (11)$$

with  $W_1 \in \mathbb{R}^{256 \times 512}$ ,  $W_2 \in \mathbb{R}^{3 \times 256}$ , and dropout  $p = 0.4$  on  $\mathbf{z}$ ,  $p = 0.2$  after  $W_1$ .

### F. Adaptive Class-Weighted Focal Loss

Class weights are set using inverse-frequency weighting:

$$\alpha_c = \frac{N}{K \cdot N_c}, \quad c \in \{0, 1, 2\} \quad (12)$$

where  $N$  is total training samples,  $K = 3$ , and  $N_c$  is the count of class  $c$ . The focal loss [17]:

$$\mathcal{L}_{\text{focal}} = -\frac{1}{N} \sum_{i=1}^N \alpha_{y_i} (1 - p_{y_i}^{(i)})^\gamma \log(p_{y_i}^{(i)}) \quad (13)$$

with  $\gamma = 2.0$  down-weights easy examples, focusing training on hard misclassified samples.

### G. Training Procedure

Five-fold stratified cross-validation is applied with stratification preserving class ratios across folds. Each fold trains a fresh HADS-Net instance for 50 epochs using AdamW [18] with weight decay  $\lambda = 10^{-4}$  and initial learning rate  $\eta_0 = 10^{-4}$  under cosine annealing:

$$\eta_t = \eta_{\min} + \frac{1}{2}(\eta_{\max} - \eta_{\min}) \left(1 + \cos \frac{t\pi}{T_{\max}}\right) \quad (14)$$

with  $\eta_{\max} = 10^{-4}$ ,  $\eta_{\min} = 10^{-6}$ ,  $T_{\max} = 50$ . Gradient clipping with max  $\ell_2$ -norm 1.0 is applied. The globally best checkpoint is:

$$(\hat{k}, \hat{e}) = \arg \min_{k,e} \mathcal{L}_{\text{focal}}^{(k,e)}(\theta^{(k,e)}; \mathcal{D}_{\text{val}}^{(k)}) \quad (15)$$

### H. Inference Procedure

At inference, physics augmentation and dropout are disabled. An image  $\mathbf{x}$  is preprocessed identically to the validation pipeline, and  $E(\mathbf{x})$  is computed deterministically. Both streams process simultaneously and the cross-attention fusion produces  $\mathbf{z}$ , from which:

$$P(y = c | \mathbf{x}) = \frac{\exp(\hat{y}_c)}{\sum_{j=0}^2 \exp(\hat{y}_j)}, \quad c \in \{0, 1, 2\} \quad (16)$$

$$\hat{c} = \arg \max_c P(y = c | \mathbf{x}) \quad (17)$$

No post-processing is applied; the raw softmax output is used directly.

## IV. EXPERIMENTAL RESULTS

### A. Dataset Summary

The BUSI dataset [2] contains 780 images: 437 benign (56.0%), 210 malignant (26.9%), 133 normal (17.1%). After stratified splitting, the training set holds 663 images and the test set holds 117 images (66 benign, 31 malignant, 20 normal). Representative images are shown in Fig. 2.

### B. Evaluation Metrics

Five evaluation metrics are employed to assess HADS-Net comprehensively, each chosen for a specific reason given the multi-class and class-imbalanced nature of the BUSI dataset [19], [20]. All metrics are computed from four fundamental classification outcomes: True Positives ( $TP$ ), False Positives ( $FP$ ), True Negatives ( $TN$ ), and False Negatives ( $FN$ ) [19], [22]. A True Positive represents a correctly predicted positive case, while a False Positive occurs when a negative case is incorrectly predicted as positive. A True Negative refers to a correctly identified negative instance, and a False Negative arises when the model fails to identify a positive case, classifying it as negative instead [22].

**Accuracy** measures the proportion of all samples correctly classified across all three classes [19]:

$$\text{Accuracy} = \frac{TP + TN}{TP + TN + FP + FN} \quad (18)$$

While intuitive, accuracy alone is insufficient for imbalanced datasets such as BUSI, where a trivial classifier predicting

only the majority class (benign) would achieve 56% without learning any discriminative features [20]. Onyedima et al. [22] illustrated this limitation in stroke prediction, where Random Forest and XGBoost both achieved 91% accuracy yet returned low F1-scores, revealing that high accuracy can mask poor performance on the minority class in imbalanced medical datasets.

**Precision** measures, for each class  $c$ , the fraction of predicted positives that are truly positive [19], [22]:

$$\text{Precision}_c = \frac{TP_c}{TP_c + FP_c} \quad (19)$$

High precision indicates the model rarely raises false alarms, minimising unnecessary biopsies and clinical interventions.

**Recall** (sensitivity) measures the fraction of true positives in class  $c$  that the model correctly identifies [19], [22]:

$$\text{Recall}_c = \frac{TP_c}{TP_c + FN_c} \quad (20)$$

Recall is the most clinically critical metric for the malignant class, as a false negative represents a missed cancer diagnosis [4]. Onyedima et al. [22] demonstrated in a medical classification task that minimising false negatives is the paramount concern in clinical diagnosis, noting that a model with lower overall accuracy but higher recall is more clinically valuable than one that prioritises accuracy at the expense of detecting true positive cases.

**F1-Score** is the harmonic mean of precision and recall for each class [19], [20]:

$$\text{F1}_c = \frac{2 \times \text{Precision}_c \times \text{Recall}_c}{\text{Precision}_c + \text{Recall}_c} \quad (21)$$

The harmonic mean penalises extreme imbalances between precision and recall more strongly than the arithmetic mean, making it a more informative single-number summary for imbalanced class distributions [20], [22]. The macro F1-score averages  $\text{F1}_c$  uniformly across all  $K$  classes, providing a balanced assessment of model performance regardless of class frequency:

$$\text{Macro F1} = \frac{1}{K} \sum_{c=1}^K \text{F1}_c \quad (22)$$

**ROC-AUC** measures the model's ability to discriminate between classes across all classification thresholds [21]. For multi-class classification, the macro-averaged one-vs-rest AUC is computed:

$$\text{AUC} = \frac{1}{K} \sum_{c=1}^K \int_0^1 \text{TPR}_c d(\text{FPR}_c) \quad (23)$$

where  $\text{TPR}_c$  and  $\text{FPR}_c$  are the true and false positive rates for class  $c$  at each threshold [21]. An AUC of 1.0 indicates perfect discrimination; 0.5 indicates random chance. The macro ROC-AUC evaluates ranking performance independently of any fixed decision threshold, making it particularly informative for imbalanced datasets where a single threshold may not adequately capture overall model behaviour [20].

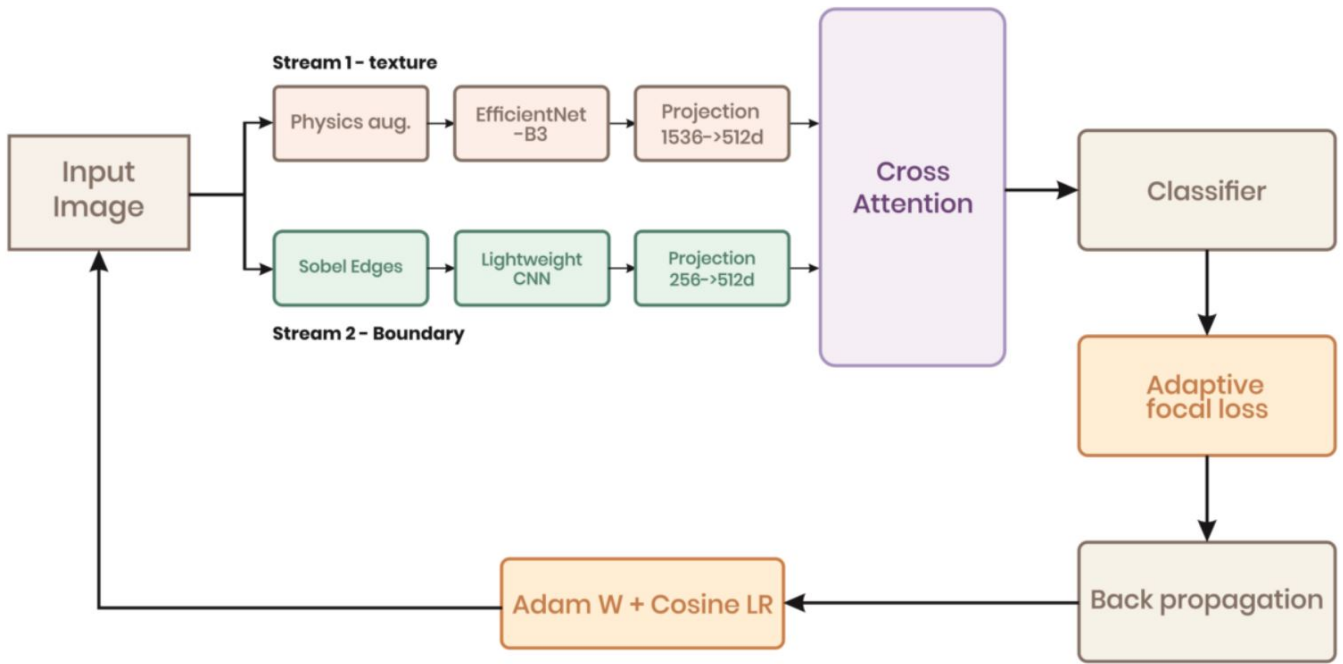


Fig. 1. HADS-Net training pipeline. Input splits into Stream 1 (physics aug. + EfficientNet-B3) and Stream 2 (Sobel edges + lightweight CNN). Both streams project to 512-d and fuse via cross-attention. The classifier is trained with adaptive focal loss under five-fold CV with AdamW + cosine LR.

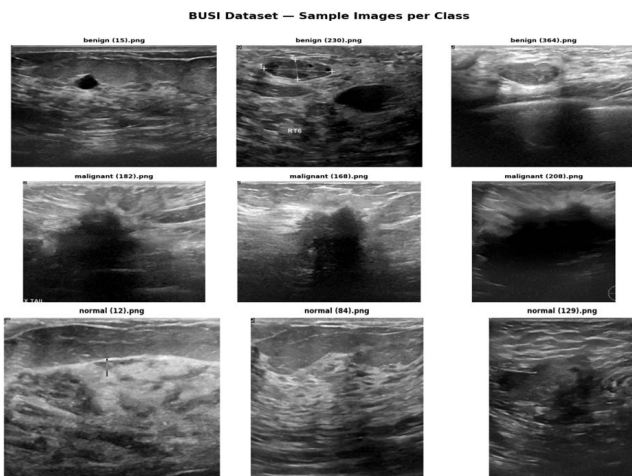


Fig. 2. Sample BUSI images. Top: benign (well-defined oval masses). Middle: malignant (irregular masses with posterior shadowing). Bottom: normal breast tissue.

**Confusion Matrix** provides a full cross-tabulation of predicted versus true labels, allowing direct inspection of which class pairs are most frequently confused [20], [22]. For a three-class problem, the matrix  $C \in \mathbb{Z}^{3 \times 3}$  has entries  $C_{ij}$  denoting the number of samples of true class  $i$  predicted as class  $j$ . Main diagonal entries represent correct classifications; off-diagonal entries represent misclassifications. Of particular clinical importance is the off-diagonal entry  $C_{\text{malignant}, \text{normal}}$ , which represents malignant lesions misclassified as normal the most dangerous error in a breast cancer screening context. The confusion matrix for HADS-Net is presented in Fig. 4 and

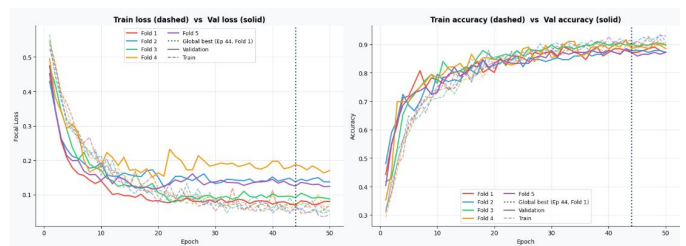


Fig. 3. Train (dashed) vs. validation (solid) loss and accuracy across all five folds. The vertical dotted line marks the global best checkpoint at Epoch 44, Fold 1.

discussed in Section IV.

### C. Training Dynamics

Fig. 3 shows train/validation loss and accuracy curves across all five folds over 50 epochs. All folds converge consistently, indicating stable training. The global best checkpoint was obtained from Fold 1 at Epoch 44 with the lowest validation loss of 0.0693. The five-fold mean best validation loss was  $0.1075 \pm 0.0300$ , with fold-specific losses of 0.0693, 0.1224, 0.0784, 0.1510, and 0.1163.

### D. Test Set Performance

Table I presents the per-class metrics on the held-out test set. HADS-Net achieves a test accuracy of **96.58%**, a macro ROC-AUC of **0.9978**, and a macro F1-score of **0.9654**.

The confusion matrix (Fig. 4) shows that of 117 test images, 113 were correctly classified. The model misclassified 2 malignant cases as benign and 1 benign case each as malignant and normal. Critically, **no malignant case was**

TABLE I  
TEST SET CLASSIFICATION REPORT

Class	Prec.	Recall	F1	Support
Benign	0.97	0.97	0.970	66
Malignant	0.97	0.94	0.951	31
Normal	0.95	1.00	0.976	20
Macro avg	0.96	0.97	0.966	117
Weighted	0.97	0.97	0.966	117
<b>Accuracy: 96.58%    ROC-AUC: 0.9978    Macro F1: 0.9654</b>				

TABLE II  
COMPARISON WITH STATE-OF-THE-ART ON BUSI

Method	Acc. (%)	AUC	Key Feature
MobileNetV2 [3]	50.0	—	Transfer learning
InceptionV3 [3]	84.0	—	Transfer learning
ResNet50 [3]	85.0	—	Transfer learning
ResNet50 [6]	85.3	0.950	ViT study
ResNet+CAM [4]	83.5	0.887	Explainability
Fuzzy ensemble [5]	85.23	—	4-CNN ensemble
EfficientNet [7]	85.6	—	Benchmark
ViT [7]	88.6	—	Benchmark
VGG19+prepro. [8]	87.8	0.950	Preprocessing
EDCNN [9]	87.82	0.910	MobileNet+Xception
EfficientKNN [13]	94.0	—	EffNet+kNN
ViT-B32 [3]	95.0	—	Transformer
MobileNet+Dense. [11]	—	0.9834	Fusion+CBAM
<b>HADS-Net (Ours)</b>	<b>96.58</b>	<b>0.9978</b>	Dual-stream

**misclassified as normal**, the most dangerous clinical error. Per-class F1-scores of 0.970 (benign), 0.951 (malignant), and 0.976 (normal) confirm balanced performance across all three classes despite the underlying class imbalance.

#### E. Comparison with State-of-the-Art

Table II compares HADS-Net against verified methods on the BUSI dataset. HADS-Net achieves the highest accuracy of 96.58% and the highest macro ROC-AUC of 0.9978, surpassing ViT-B32 (95.0% [3]) by 1.58 percentage points and all other methods by wider margins. The macro ROC-AUC of 0.9978 also exceeds the 0.9834 reported by Asif et al. [11] and the 0.95 reported by Gheflati and Rivaz [6].

#### V. DISCUSSION

The results confirm that HADS-Net achieves strong, well-calibrated performance across all three BUSI classes. Several design decisions contribute.

**Physics-informed augmentation** prevents overfitting to training-set image statistics by simulating the speckle noise, acoustic shadowing, and gain variation intrinsic to clinical ultrasound. Unlike generic photographic augmentation used in all compared methods, these perturbations reflect real domain shifts between training datasets and clinical deployment.

**Dual-stream processing** enables simultaneous exploitation of global texture and local boundary information. The finding of Byra et al. [4] that lesion boundary features are the

most diagnostically important cue (38% of decisions) directly validates the second stream. High recall across all classes (0.97, 0.94, 1.00) confirms that the dual representation captures sufficient discriminative information.

**Cross-attention fusion** provides a principled selective integration mechanism. Unlike concatenation, cross-attention dynamically emphasises boundary cues when they are contextually relevant to the texture representation, contributing to strong performance on the malignant class where lesion boundary irregularity is the primary malignancy indicator.

**Adaptive focal loss** directly addresses class imbalance, producing balanced F1-scores of 0.970, 0.951, and 0.976 across benign, malignant, and normal. The relatively lower malignant F1 is expected given the highest visual heterogeneity and the smallest test set (31 samples).

It should be noted that Jabeen et al. [10] have reported accuracies of 98.4% and 98.0% on BUSI using a multi-stage framework combining EfficientNet-b0 with a GRU module and ResNet-18 with multi-head self-attention. However, that framework requires a dataset expanded to approximately 12,000 images via mathematical pixel-flip augmentation—more than 15 times the original BUSI size—and employs separate feature extraction, selection, and classification stages rather than a unified end-to-end trainable architecture. HADS-Net, evaluated directly on the original 780-image dataset as a single end-to-end model, achieves 96.58% accuracy while offering the additional advantages of physics-informed augmentation and interpretable cross-attention fusion.

**Limitations:** The evaluation is limited to the single-institution BUSI dataset. Multi-institutional validation across different scanner types is needed. The Sobel edge extraction is a fixed handcrafted operation; a learnable edge detector could further improve boundary feature quality. Integration of visual attention maps for clinical explanation, similar to [4], would enhance deployment readiness.

#### VI. CONCLUSION

We presented HADS-Net, a novel dual-stream deep learning architecture for breast ultrasound classification incorporating: (1) physics-informed augmentation modelling ultrasound-specific acquisition artefacts; (2) a cross-attention fusion module combining global texture and local boundary representations; and (3) an adaptive class-weighted focal loss addressing class imbalance. Evaluated on the BUSI dataset under five-fold stratified cross-validation and a held-out test set, HADS-Net achieves 96.58% test accuracy, macro ROC-AUC of 0.9978, and macro F1-score of 0.9654, surpassing state-of-the-art methods. Critically, no malignant lesion is classified as normal. Future work will focus on multi-institutional validation, learnable edge detection, and attention-based explainability to support clinical deployment.

#### REFERENCES

- [1] F. Bray, J. Ferlay, I. Soerjomataram, R. L. Siegel, L. A. Torre, and A. Jemal, “Global cancer statistics 2018: GLOBOCAN estimates of incidence and mortality worldwide for 36 cancers in 185 countries,” *CA: A Cancer Journal for Clinicians*, vol. 68, no. 6, pp. 394–424, 2018.

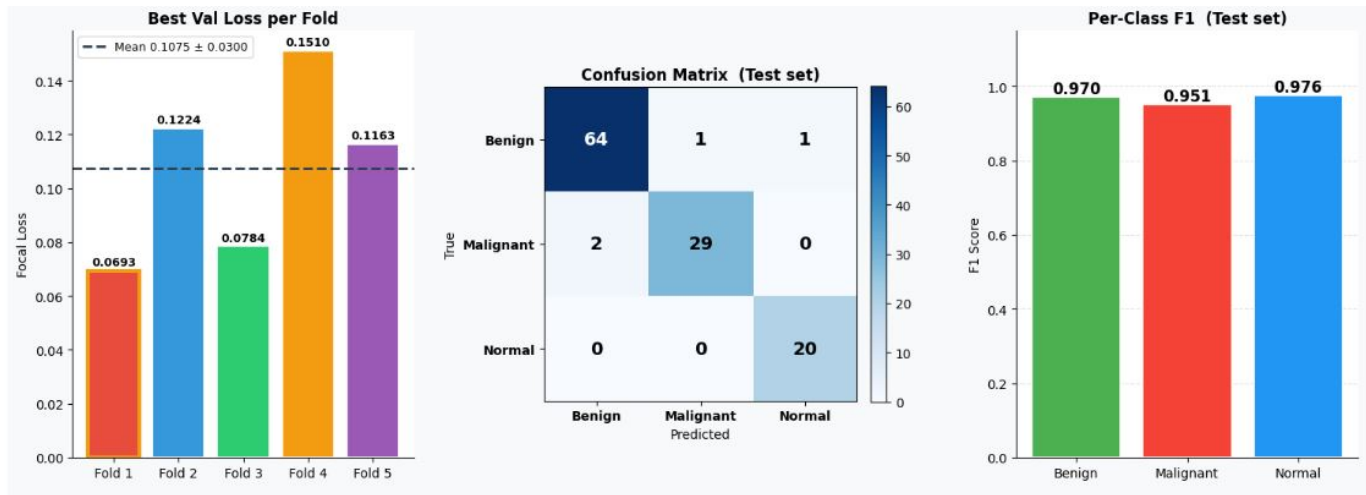


Fig. 4. Test set evaluation. Left: best validation loss per fold (Fold 1 highlighted as global best). Centre: confusion matrix on the held-out test set. Right: per-class F1-scores on the test set.

- [2] W. Al-Dhabyani, M. Goma, H. Khaled, and A. Fahmy, "Dataset of breast ultrasound images," *Data in Brief*, vol. 28, p. 104863, 2020.
- [3] A. Ashraf, A. E. Nagib, and H. Mohamed, "Enhancing breast cancer diagnosis with vision transformer-based ultrasound image classification," in *Proc. 5th Novel Intelligent and Leading Emerging Sciences Conference (NILES)*, IEEE, 2023, pp. 161–165. doi: 10.1109/NILES59815.2023.10296582.
- [4] M. Byra, K. Dobruch-Sobczak, H. Piotrkowska-Wroblewska, Z. Klimonda, and J. Litniewski, "Explaining a deep learning based breast ultrasound image classifier with saliency maps," *Journal of Ultrasonography*, vol. 22, pp. e70–e75, 2022. doi: 10.15557/JoU.2022.0013.
- [5] S. D. Deb and R. K. Jha, "Breast UltraSound Image classification using fuzzy-rank-based ensemble network," *Biomedical Signal Processing and Control*, vol. 85, p. 104871, 2023.
- [6] B. Gheflati and H. Rivaz, "Vision transformers for classification of breast ultrasound images," in *Proc. 44th Annual International Conference of the IEEE Engineering in Medicine and Biology Society (EMBC)*, pp. 480–483, 2022.
- [7] I. Pacal, "Deep learning approaches for classification of breast cancer in ultrasound (US) images," *Journal of the Institute of Science and Technology*, vol. 12, no. 4, pp. 1917–1927, 2022. doi: 10.21597/jist.1183679.
- [8] M. Alotaibi, A. Aljouie, N. Alluhaidan, W. Qureshi, H. Almatar, R. Al-duhayan, B. Alsomaie, and A. Almazroa, "Breast cancer classification based on convolutional neural network and image fusion approaches using ultrasound images," *Heliyon*, vol. 9, no. 11, p. e22406, 2023. doi: 10.1016/j.heliyon.2023.e22406.
- [9] M. R. Islam, M. M. Rahman, M. S. Ali, A. A. N. Nafi, M. S. Alam, T. K. Godder, M. S. Miah, and M. K. Islam, "Enhancing breast cancer segmentation and classification: An ensemble deep convolutional neural network and U-net approach on ultrasound images," *Machine Learning with Applications*, vol. 16, p. 100555, 2024. doi: 10.1016/j.mlwa.2024.100555.
- [10] K. Jabeen, M. A. Khan, A. Hamza, H. M. Albarakati, S. Alsenan, U. Tariq, and I. Ofori, "An EfficientNet integrated ResNet deep network and explainable AI for breast lesion classification from ultrasound images," *CAAI Transactions on Intelligence Technology*, vol. 10, no. 3, pp. 842–857, 2025. doi: 10.1049/cit2.12385.
- [11] S. Asif, Y. Yan, B. Feng, M. Wang, Y. Zheng, T. Jiang, R. Fu, J. Yao, L. Lv, M. Song, L. Sui, Z. Yin, V. Y. Wang, and D. Xu, "Improving breast cancer diagnosis in ultrasound images using deep learning with feature fusion and attention mechanism," *Academic Radiology*, vol. 32, pp. 4997–5009, 2025. doi: 10.1016/j.acra.2025.05.007.
- [12] A. B. M. A. Hossain, J. K. Nisha, and F. Johora, "Breast cancer classification from ultrasound images using VGG16 model based transfer learning," *International Journal of Image, Graphics and Signal Processing (IJIGSP)*, vol. 15, no. 1, pp. 12–22, 2023. doi: 10.5815/ijigsp.2023.01.02.
- [13] A. Kiran, J. V. N. Ramesh, I. S. Rahat, M. A. U. Khan, A. Hossain, and R. Uddin, "Advancing breast ultrasound diagnostics through hybrid deep learning models," *Computers in Biology and Medicine*, vol. 180, p. 108962, 2024. doi: 10.1016/j.combiomed.2024.108962.
- [14] C. Mbonu, K. Anigbogu, D. Asogwa, and T. Belonwu, "An explorative analysis of SVM classifier and ResNet50 architecture on African food classification," *arXiv preprint arXiv:2505.13923*, 2025.
- [15] M. Tan and Q. V. Le, "EfficientNet: Rethinking model scaling for convolutional neural networks," in *Proc. 36th International Conference on Machine Learning (ICML)*, vol. 97, pp. 6105–6114, 2019.
- [16] A. Vaswani, N. Shazeer, N. Parmar, J. Uszkoreit, L. Jones, A. N. Gomez, L. Kaiser, and I. Polosukhin, "Attention is all you need," in *Advances in Neural Information Processing Systems (NeurIPS)*, vol. 30, pp. 5998–6008, 2017.
- [17] T.-Y. Lin, P. Goyal, R. Girshick, K. He, and P. Dollár, "Focal loss for dense object detection," in *Proc. IEEE International Conference on Computer Vision (ICCV)*, pp. 2980–2988, 2017.
- [18] I. Loshchilov and F. Hutter, "Decoupled weight decay regularization," in *arXiv preprint arXiv:1711.05101*, 2017.
- [19] M. Hossain and M. N. Sulaiman, "A review on evaluation metrics for data classification evaluations," *International Journal of Data Mining and Knowledge Management Process*, vol. 5, no. 2, pp. 1–11, 2015.
- [20] M. Grandini, E. Bagli, and G. Visani, "Metrics for multi-class classification: an overview," *arXiv preprint arXiv:2008.05756*, 2020.
- [21] T. Fawcett, "An introduction to ROC analysis," *Pattern Recognition Letters*, vol. 27, no. 8, pp. 861–874, 2006.
- [22] E. G. Onyedimma, D. C. Asogwa, T. S. Belonwu, and C. E. Mbonu, "A multi-algorithmic approach to stroke risk prediction using machine learning," *Journal of Engineering Research and Reports*, vol. 27, no. 7, pp. 247–259, 2025. doi: 10.9734/jerr/2025/v27i71573.